5.4 Toward the Estimation of the Refractive Index Gradient from Clear Air Wind Profiler Echoes

Catherine Gaffard[*] [1], Laura Bianco [2], Monica Matabuena [3], Vlasdisvlas Klaus [4]

[1] Met Office, Meteorology Building, PO Box 243, Earley Gate, University of Reading, RG6 6BB, UK (corresponding author)
[2] CETEMPS - Centre of Excellence, University of L'Aquila, Italy
[3] Group of environmental Engineering. School of Engineering of Bilbao, Spain
[4] CNRM, Meteo-France Toulouse, France

1. INTRODUCTION

Wind profilers have been primarily designed to provide measurement of the wind; they also contain information about temperature and humidity vertical distribution (Furumoto et al. 2003). The information is derived from the first three moments of the measured Doppler spectra (Gossard 1982, 1998). Several works showed that wind profiler data in the boundary layer, combined with passive instrument like microwave radiometer, can be used to evaluate humidity profile (Bianco et al. 2005), or humidity gradient profile (Stankov et al. 2003).
This paper describes some investigations done on wind profiler data quality in order to know if they can be used to detect and quantify change in the refractive index. Section 2 describes the site and instrumentation used in this study. Section 3 looks at the consistency of the signal between beams. Section 4 compares the signal to noise ratio with the refractive index gradient. Finally, section 5 summarises the results.

2. INSTRUMENTATION

The dataset used for this study has been collected during the international COST 720 Temperature, hUmidity and Cloud (TUC) profiling experiment. This experiment was organized during three months (November to February) in winter 2003-2004 at Payerne, Switzerland. Various *in situ* and active/passive ground-based remote sensing systems, including three microwave radiometers, a cloud radar, a wind profiler and radiosondes were operating in the same location.

The wind profiler is a LAP-3000 manufactured by Vaisala (ex Radian). The operating frequency is 1290 MHz. This radar operates in pulse mode, using three beams (one vertical and two oblique). It is configured to operate in two modes (low mode and high mode), which correspond to two different vertical resolutions (respectively 45 and 210 m) and two different vertical ranges (respectively from 135 to 1035 m, and from 675 to 4975 m). The two modes are interlaced in time. A dwell time of 35 s is used to get the data from each pointing beam. Thus, three and half minute elapse before the system returns to the beginning of its sequence. The LAP-3000 system offers the possibility to save the raw data (i.e.: averaged Doppler spectra) as well as the moment data, computed with the Vaisala Single Peak algorithm.

The radiosondes used in this comparison are the operational Suisse radiosonde SRS. They report temperature, humidity and wind vector measurements. The height sampling is variable, around 30 m for temperature and humidity, 40 m to a couple of hundred meters for the wind.

3. VARIABILTY AND CONSISTENCY BETWEEN BEAM

In this section, the variability between the three beams of the signal to noise ratio and the Doppler width is examined. The data used are the moments computed and archived at the highest time resolution by

[*] Corresponding author: Catherine.gaffard@metoffice.gov.uk

the manufacturer software. This software computes the three moments for every range gate, even if there is no detectable atmospheric signal. So, before doing any analysis, some quality control has to be applied.

3.1. Atmospheric signal identification

During the TUC field experiment, a building site was set up at around 300 m from the radar site. A couple of cranes were in action. A direct reflection of the emitted power by some of the cranes has been picked up through a side lobe of the antenna. The three beams are picking this signal. When the crane is not moving the direct reflection create a signal with no Doppler shift which is removed by the ground clutter algorithm, while it is not the case when the crane is moving. In Figure 1 is plotted the signal to noise ratio of the vertical beam. This shows clearly the impact of the crane during the working hour. A rectangular pattern of increase signal starting at 07:00 UTC, finishing at 16:00 UTC with a gap of 1hour at 11:00 UTC, with a vertical extension around 200 m starting at around 200 m above the ground, is present on nearly every working days. The gap in the middle of the day coincides with lunch break. Data below 400 m during working time are likely to be contaminated by the crane signal. Beside the fact this signal coincides with working hours, it is rather difficult to identify it. There is no obvious discontinuity in the wind field, (crane are only working in low wind condition) nor special spectral characteristics.

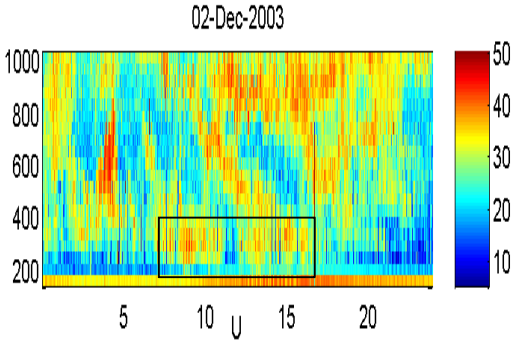

Figure 1: Range corrected signal to noise ratio versus time. The signal inside the box is due to direct reflection to the crane, the lunch break is visible from 11:00 to 12:00 UTC. Atmospheric signal can also overlap the crane signal.

Data with a signal to noise lower than 15dB were not considered. To reject rain and drizzle situations, a check on the persistence of the negative wind speed has been used. Time and space continuity were also used to reject unrealistic data, a last check on the width was used to reject too narrow peaks and too wide peaks. The minimum width corresponds to beam broadening effect. This effect is purely geometrical and linked to the beam aperture or beam width. For a constant wind, the projection of the wind vector onto the radial direction within the beam is changing; each contribution to the Doppler spectrum is weighted accordingly to the illumination pattern of the antenna. The Doppler width is then related to the beam width and the horizontal speed. If a shear in the speed exists within the volume of resolution, the radial contribution of the wind is also changing within the beam and will contribute, accordingly to the illumination pattern of the antenna, to the Doppler spectrum. This broadening is fully described in Doviak and Zrnic (1984) and referenced as shear broadening effect. The formulation of σ^2_{shear} (2^{nd} moment of the shear broadening) given in Doviak and Znirc has been adapted to wind profiler geometry by Jacoby et al. (2002) and is used in this study to correct the 2^{nd} moment of the Doppler spectrum from the shear broadening effect:

Eqn. 1

$$\sigma_{shear}^{\ 2} = k_\beta^2 + k_\theta^2 + k_h^2$$

$$k_\beta = \sigma_\beta (u\cos\beta - v\sin\beta)$$

$$k_\theta = \sigma_\theta [r\cos^2\theta(\sin\beta\partial u/\partial z + \cos\beta\partial v/\partial z) - u\sin\beta\sin\theta - v\cos\beta\sin\theta + r\cos\theta\sin\theta\partial w/\partial z + w\cos\theta]$$

$$k_h = \sigma_r [\cos\theta\sin\theta(\sin\beta\partial u/\partial z + \cos\beta\partial v/\partial z) + \sin^2\theta\partial w/\partial z]$$

k_β, k_θ, k_r are the components of the radial shear in the spherical coordinate system where β is the azimuth of the antenna (relative to the north), θ the elevation angle from the ground (90 degrees for the vertical beam). r is the range of the target, $(\sigma_\beta)^2$, $(\sigma_\theta)^2$ are the second moments of the two-way antenna power angular pattern in the indicated direction (β, θ) and σ_r^2 is the second moment of the range weighting power function in the radial direction, which is a function of the pulse shape and the receiver characteristic.

For a circular symmetric Gaussian pattern we have:

$\sigma_\beta = \sigma_\theta = \Phi/(4\sqrt{\log(2)})$ where Φ is the one way half-power width.

For a rectangular impulsion and a Gaussian receiver under matched condition (Doviak and Znirc 1984)

$\sigma_r = (0.35c\ \tau/2)$ where τ is the impulsion length.
The impulsion used by the wind profiler in this study is pretty close to a square impulsion, and the characteristic of the receiver can be approximate to a Gaussian filter.
The minimum width will correspond to situation with no shear in the wind. Width versus wind speed is plotted in Figure 2. The Doppler spectral width, given in the raw file, is twice the square root of the 2nd moment of the spectrum.

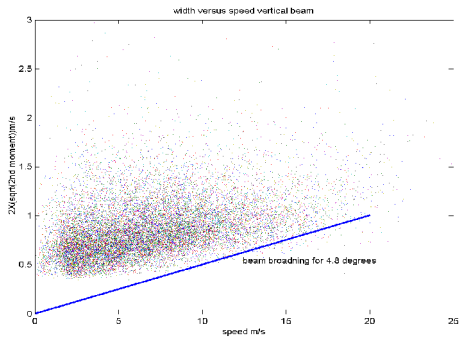

Figure 2: Width versus wind speed for the vertical beam, the blue line is the expected beam width broadening.

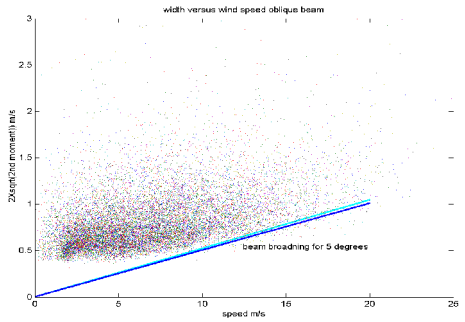

Figure 3: Width versus wind speed for the oblique beam, blue and cyan lines are the expected beam width broadening (geometrical effect of different wind orientation - blue and cyan colour - has been taken into account).

To obtain this plot previous quality controls have been used with strong constraint in the consistency of the speed in space and in time. This last test might restrict to stationary situations, but it is rejecting a lot of aberrant data and will certainly not affect the minimum broadening we are interested in at this stage. The minimum envelop of the scatter plot corresponds very well with the expected value and this is for the three beams, so we can assume than the beam width stated by the manufacturer is right. For the vertical beam the minimum width is slightly wider than expected, but the minimum envelope is parallel to the expected value. This bias in the width for the vertical beam will be detailed in the next chapter. Only spectra with a width wider than the beam broadening width have been selected. The other factor affecting the 2nd moment of spectrum ($\sigma_{spec}^{\ 2}$) is linked to the turbulence (σ^2_{turb}) by:

$$\sigma_{spec}^{\ 2} = \sigma^2_{turb} + \sigma^2_{shear}$$

Several works have shown that it might be possible to characterize the intensity of the turbulence by using the spectral width of the Doppler spectrum (Frish and Clifford 1974, Gossard 1998, White 1999, Jacoby et al. 2001).

At the opposite, a very wide spectrum can be due to bird or rain contamination. The climatology of eddy dissipation rate is not well known at a time scale of 30 s. Recent observations done by a cloud radar at Chilbolton reveal that strong values of the eddy dissipation rate ε (0.005 m^2/s^3) can be found in stratocumulus. The expected width derived from this dissipation rate using the White formula (Eqn. 2) and the beam broadening effect for the low and high mode (Eqn. 1) are shown in Figure 4 and Figure 5.

Eqn. 2

$$\varepsilon = \sigma_{turb}^3 (4\pi / \alpha_e)^{3/2} J^{-3/2}$$

$$J = 12\Gamma(2/3). \int_0^{\pi/2} \int_0^{\pi/2} (\sin^3\theta)(\sigma_h^2 \cos^2\theta + \sigma_b^2 \sin^2\theta + (L^2/12)\sin^2\theta\cos^2\phi)^{1/3} d\theta d\phi$$

Where:

$\sigma_b = r\sigma_\theta$
$L = vT$

v is the horizontal speed corresponding to the integration time T.
$\alpha_e = 1.6$

The highest envelope of these two scatter plots have been used as a limit for the broadening for the modes.

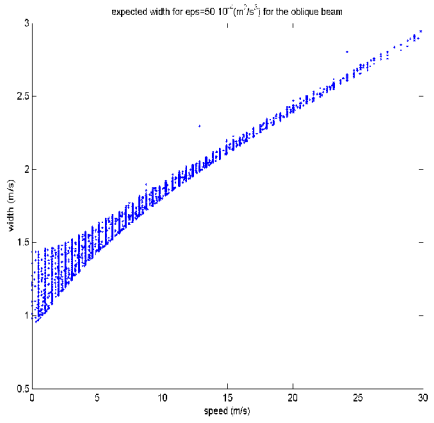

Figure 4: Expected width for ε=0.005 m^2/s^3 for different gates versus radiosonde wind speed, for the low mode.

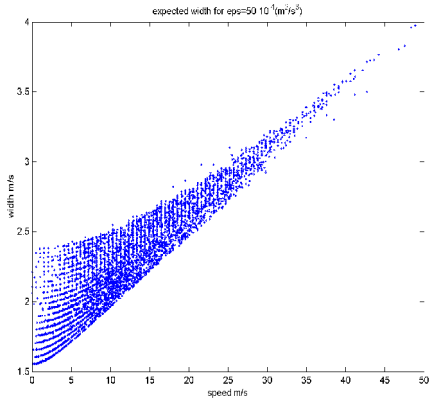

Figure 5: Expected width for ε=0.005 m^2/s^3 for different gates versus radiosonde wind speed, for the high mode.

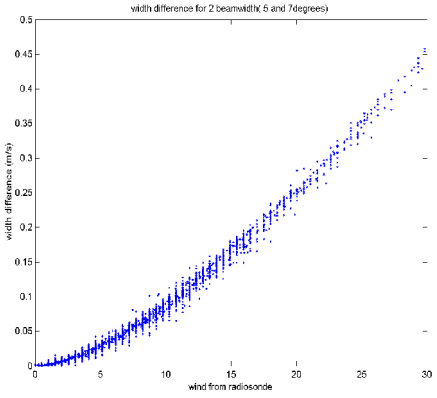

Figure 6: Width difference for two beamwidths (one way half power width 5 and 7 degree) for ε=0.002 m^2/s^3, for different gates versus radiosonde wind speed.

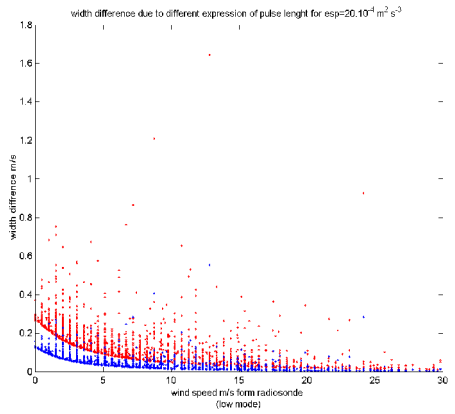

Figure 7: width difference due to different expression of σ_r for ε=0.002 m^2/s^3, for different gates versus radiosonde wind speed.
Blue points: 0.5cτ/2 - 0.35cτ/2
Red points: cτ/2 - 0.35cτ/2

For further evaluation of the turbulence, it is important to know with accuracy the volume of the illumination pattern. The beam width is an important factor and will dominate as the wind increases (Figure 6). The conversion between the pulse duration and the radial 2nd moment of the illumination pattern has also some impact on the filtering, as it can be seen in Figure 7. It will depend on the characteristic of the pulse shape and the receiver filter. Different values are found in the literature as 0.30cτ/2 (Stankov 2003) 0.35cτ/2 (Doviak and Znirk), cτ/2 (Gossard 1998).

To summarize, table 1 gives the percentage of selected data using each quality control, for the low mode and high mode.

Table 1: % of data selected using each quality control.

Quality flag	SNR> -15dB & <50dB	Vertical speed <3m/s & speed <50m	Rain flag	Width >wind broadening <max expected width	Shear in height < 0.02 and continuity in time < 6 m/s	No crane data h>400m	All together
Low mode	53%	83%	74%	49%	42%	71%	11%
High mode	26%	53%	75%	29%	18%	100%	5%

3.2. Variability and consistency between the three beams

3.2.1. Signal to Noise Ratio (SNR)

The scatter plot of the power between vertical and oblique beam is plotted on Figure 8 and Figure 9. In average there is a bias of -2.8 dB between the vertical beam and the oblique beam with a standard deviation of 4.07 dB, there is a small bias between the two oblique beams (-0.2 dB) and the standard deviation is 3.35 dB. This underestimation of the signal in the vertical beam is likely to be the result of the ground clutter removal algorithm and to the direct current removal algorithm. The ground clutter algorithm (Riddle and Angevine, 1992) identifies a symmetric signal peak centred about zero Doppler shifts, and then excludes that region for search for atmospheric signal. The algorithm is not applied if the signal at the height above was near the zero velocity. A maximum height for ground clutter search is used.

Because of the lack of signal in the highest gate, where the ground clutter is not applied, the signal processing can lock on noise away from the zero Doppler and then, if lower down the real signal is at the zero Doppler, the ground clutter algorithm will avoid the zero Doppler and will carry on locking on noise. The quality control should reject most of these data, but not all of

them. The other source of bias comes from the Direct Current (DC) algorithm removal. It removes the energy at the zero Doppler. In average, the two combined effects introduce a bias in the vertical beam power.

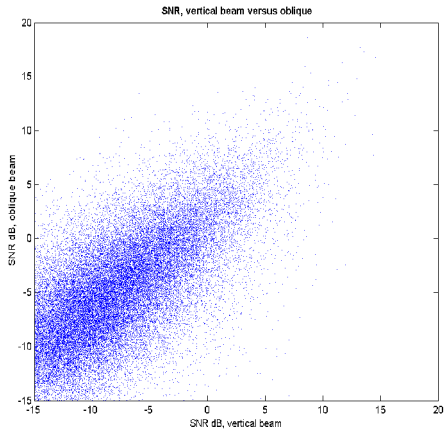

Figure 8: Vertical beam SNR (x-axis) versus oblique beam SNR (y-axis). Values are in dB and are not range corrected (low mode).

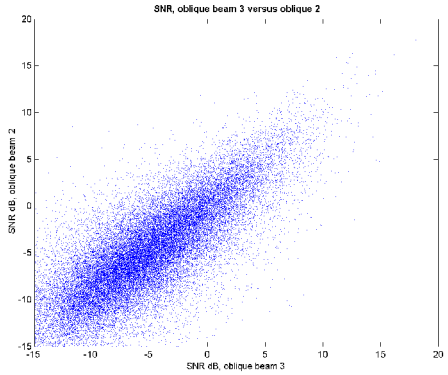

Figure 9: Oblique beam 3 SNR (x-axis) versus oblique beams 2 SNR (y-axis). Values are in dB and are not range corrected (low mode).

The histograms of the shift Doppler for the three beams are shown on Figure 10, Figure 11, Figure 12. For the vertical beam the distribution is very narrow around the zero Doppler, so the DC algorithm will mainly affect the vertical beam. For the oblique beams, the gap at the zero Doppler is the result of the combined effect of the ground clutter algorithm, which tries to avoid the zero Doppler, and the DC algorithm which removes the value at the zero Doppler, therefore reducing the possibility of having a maximum at zero. The residual bias observed between the two oblique beams could come from the fact that there is more data at the zero Doppler, therefore more biased by the DC algorithm for the oblique beam 3 (4272 data), than for the oblique beam 2 (3717data), due to prevailing wind direction.

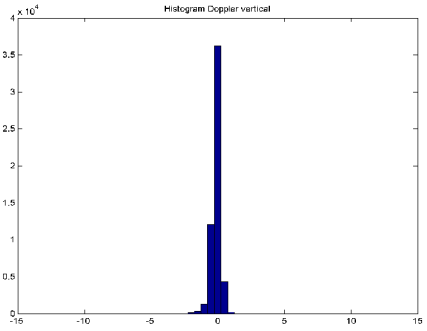

Figure 10: Histogram of the Doppler for vertical beam.

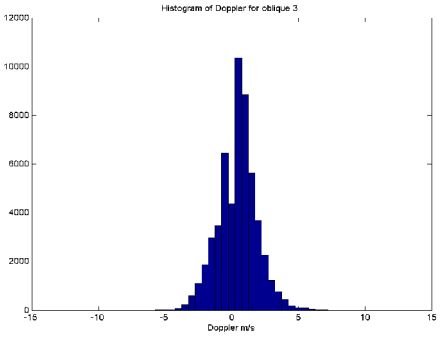

Figure 11: Histogram of the Doppler for oblique 3.

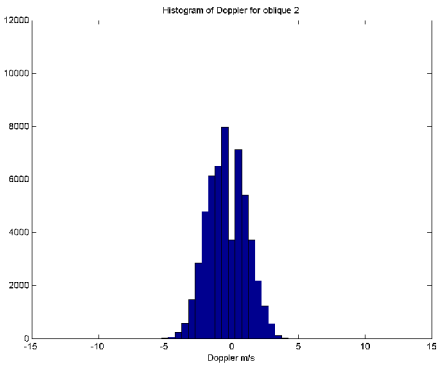

Figure 12: Histogram of the Doppler for oblique2.

The standard deviation between the values obtained from two different beams is quite high and represents nearly a factor 3 in the possible evaluation of C_n^2. Part of this variability is probably due to the instrument noise, but for values well above the noise level, the scatter plot between the two oblique beams remains wide and has to be attributed to atmospheric variability.

By averaging the data in time, the standard deviation (Figure 13) decreases sharply in the first ½ hour and less after this time. The correlation increases (Figure 14) as well sharply using ½ hour of average. The correlation between the values from the vertical beam and the oblique beam is very small and clearly indicates a problem in the vertical beam.

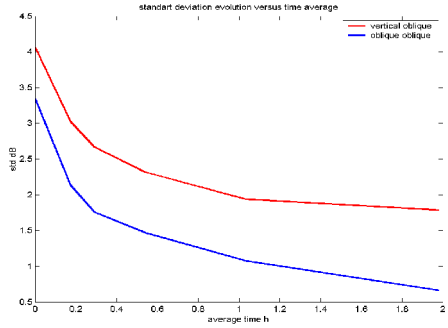

Figure 13: Standard deviation evolution versus time averaging for the SNR. Red curve indicates vertical against oblique, blue curve oblique against the other oblique (low mode).

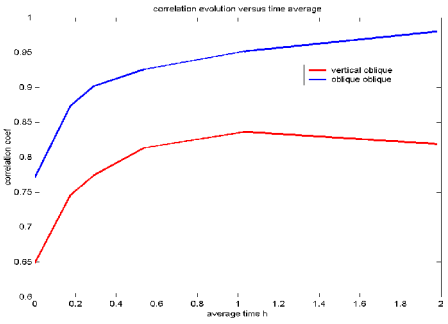

Figure 14: Same as Figure 13, but for the correlation.

3.2.2. Doppler width

Once corrected for shear broadening, the Doppler width for the three beams should represent the turbulent broadening and should be the same for the three beams. Data leading to negative width has been rejected. The scatter plots of σ^2_{turb} between vertical and oblique beams, and between the two oblique beams are shown in Figure 15 and Figure 16.

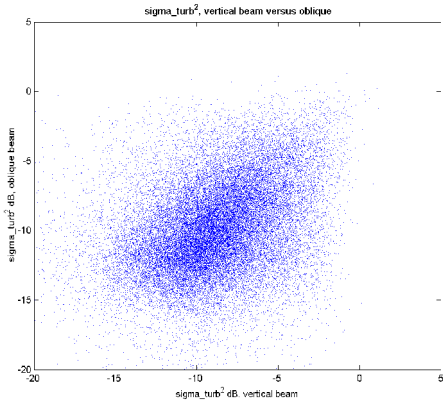

Figure 15: σ_{turb}^2 from oblique beam (y-axis) versus σ_{turb}^2 from vertical beam (x-axis).

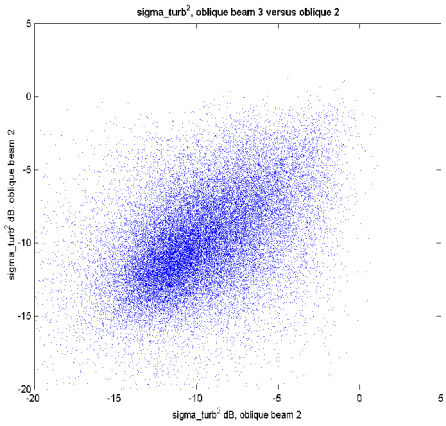

Figure 16: σ_{turb}^2 from oblique beam 3 (y-axis) versus σ_{turb}^2 from oblique beam 2 (x-axis).

The data scatter is very wide. The standard deviation between vertical and oblique is 4.1 dB and 3.87 dB for the two oblique beams. Compared to the range of variability, which is around 15 dB, the standard deviation is large. This leads to very poor correlation between σ^2_{turb} for the different beams: 0.31 for vertical and oblique beam, 0.42 for the two oblique. The results are slightly worse for the high mode with a correlation of 0.31 for vertical and oblique and 0.39 for the two oblique beams (not shown). In average, the vertical values are positively biased by 0.98 dB compared to the oblique, the bias between the oblique 3 and oblique 2 is 0.12 dB. This bias is small but significant (the statistical error for it is +/-0.017 dB). As already mentioned, the DC removal introduces a bias in the signal to noise ratio for the vertical beam and also between the two oblique beams, although much smaller than the one for the vertical beam. By taking away the power at 0 it also

artificially widens the spectrum and introduces a positive bias in the width.

There are several factors that contribute to the variability of σ^2_{turb}. As for the SNR, the instrument noise and the atmospheric variability contribute to the variability of σ^2_{turb}. Then σ^2_{turb} is corrected from the wind shear broadening which implies the knowledge of the volume resolution and the correct estimation of the Doppler shift on the three beams for two consecutive gates. The use of a simple correcting factor which takes into account only the beam broadening compared to the full correcting factor, which include the shear and the geometry of the beam, marginally degrades the correlation for the low mode and marginally improve the correlation for the high mode. This seems to indicate that the noise introduced by the correction (due to the uncertainty in the wind shear) is at the same level than the correction itself.

By averaging, the correlation increase and the standard deviation decrease sharply in the first ½ hour of average (Figure 17 and Figure 18). The correlation of σ^2_{turb} between the vertical and oblique beam is much smaller than for the two oblique beams, and the standard deviation is significantly higher than for the oblique indicating here again a contamination of the vertical beam.

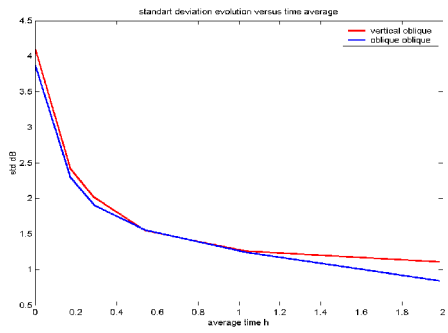

Figure 17: Standard deviation evolution versus time averaging for the width. Red curve indicates vertical against oblique beam, blue curve oblique against the other oblique (low mode).

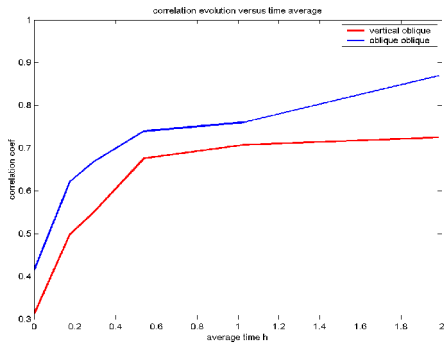

Figure 18: Correlation coefficient evolution versus time averaging for the width. Red curve indicates vertical against oblique beam, blue curve oblique against the other oblique (low mode).

These results seem to indicate that, for an evaluation of C_n^2 and of σ^2_{turb}, it is better to use the oblique beam than the vertical one. An average over ½ hour significantly reduces the dispersion between the two oblique beams. The correlation between the data, which are supposed to measure the same atmosphere, remains quite low, in particular for the width. Part of the dispersion might be due to the atmospheric variability, but most of it is due the fact that even with our quality control, erroneous data has been taken in the sampling.

4. COMPARISON WITH RADIOSONDES

4.1. Gradient of refractive index versus SNR

Wind profiler data have been collocated with the radiosonde measurements within a time window of ½ hour centred on the launch time of the radiosonde. Following Gossard (1998), the gradient of the potential refractive index has been computed from the radiosonde measurements. The potential temperature and the potential water vapour have been averaged at the radar resolution, and the potential refractive index gradient (dn/dz) has been computed from the mean values. 4 examples of comparison are shown thereafter.

Example 1:

Figure 19 shows an example of comparison between the signal to noise ratio from the oblique beam averaged over ½ hour (red line) and the $(dn/dz)^2$ (blue line) computed

from the radiosonde. The thick line has been obtained from the average of the data that have past the full quality control, as the thin line is obtained form data flagged as not rain. The values are expressed in decibel and the radiosonde curve has been empirically shifted by the same amount for all the comparison. The agreement between the two curves is very good for the low mode and the high mode.

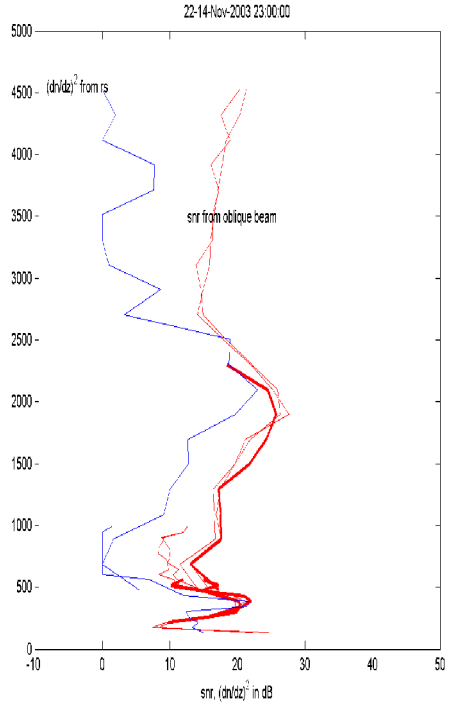

Figure 19: Profile of $(dn/dz)^2$ from radiosonde (blue line) in dB. SNR averaged over ½ hour from oblique beams in red. Thick line corresponds to quality controlled data; thin line is obtained from data flag as not rain (14/11/03).

The time height cross section of the data use in the average (Figure 20) for the high mode shows that the altitude of the strong layer is decreasing with time. Such time evolution can explain the mismatch in height for the high mode between the radiosonde and wind profiler measurements. For the low mode (Figure 21), the signal to noise ratio is quite variable, but in average the altitude of the maximum in the signal is in very good agreement with the radiosonde.

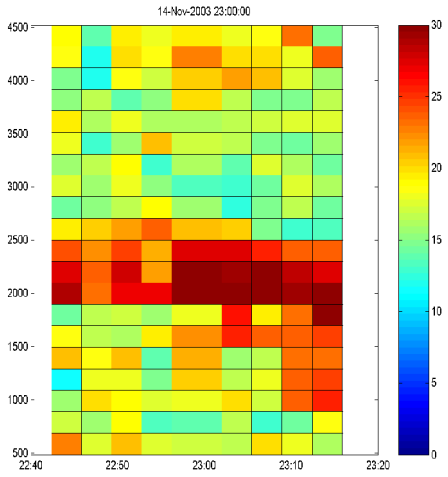

Figure 20: High time resolution time height cross section of SNR used for the ½ hour average profile. High mode (14/11/03, 23:00 UTC). Colour scale in dB

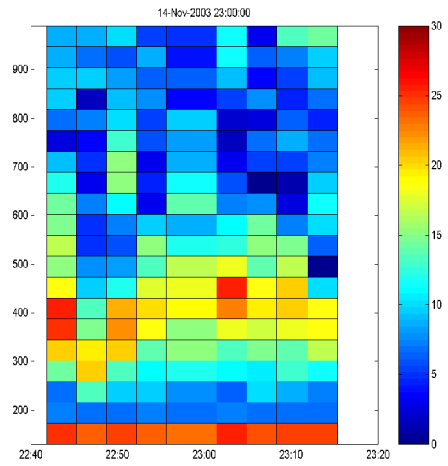

Figure 21: High time resolution time height cross section of SNR used for the ½ hour average profile. Low mode (14/11/03, 23:00 UTC). Colour scale in dB.

Example 2:

The following example shows a case where strong signal exists in the low mode while the radiosonde indicates no strong change in the refractive index. For this case there is quite a lot of fluctuation in the vertical speed (Figure 22). The temperature profile (Figure 23) shows a well-mixed layer following the dry adiabatic lapse rate.

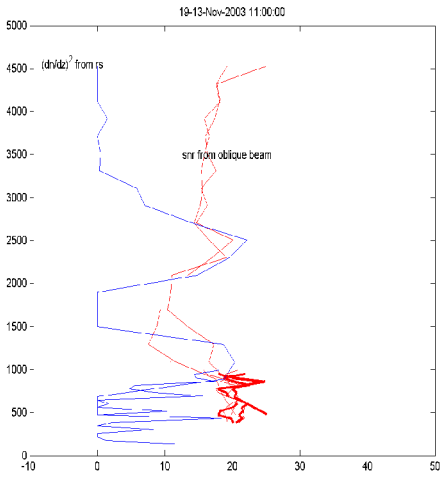

Figure 22: Same as Figure 19, but for the 13/11/03, 11:00 UTC.

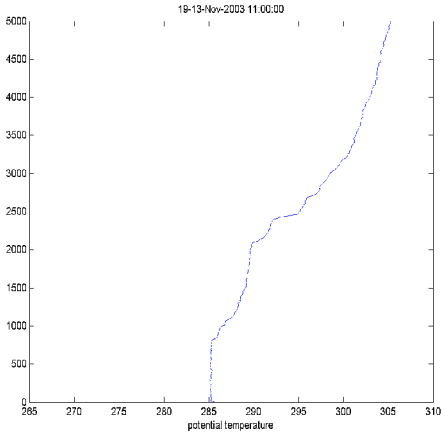

Figure 23: Potential temperature profile from radiosonde for the 13/11/03, 11:00 UTC.

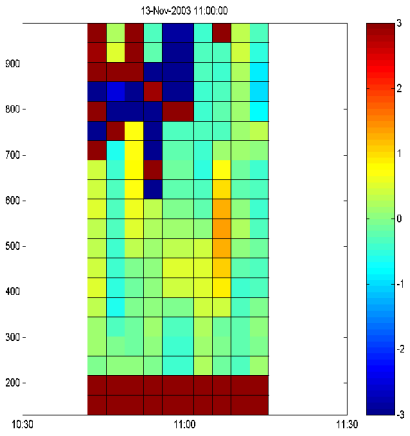

Figure 24: same as Figure 21 but for the vertical speed and for the 13/11/03, 11:00 UTC. Colour scale in m/s

Example 3:

Sometime the wind profiler shows low signal while the radiosonde indicates variations in the refractive index (Figure 25). It has to be noted that none of the data pass the quality control.

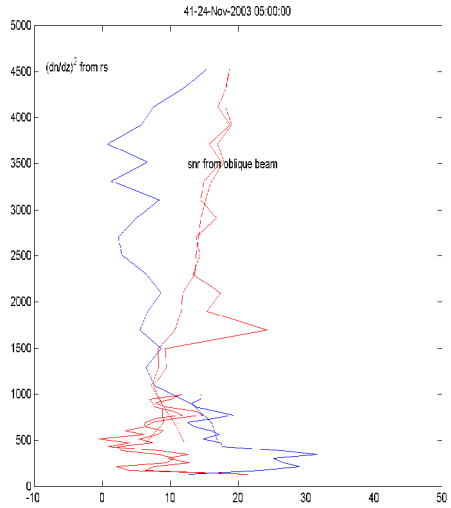

Figure 25: Same as figure 25, but for the 24/11/03, 05:00 UTC.

Example 4:

For the 19 of November the agreement is quite good again where two layers seen by the radiosonde are also seen by the wind profiler (Figure 26). Nevertheless, the time evolution of the signal shows (Figure 27) that, if the comparison was done 10 minutes latter, the amplitude of the two layers would have been completely different. Such variability shows how difficult it is to compare spot measurement (radiosonde) to radar measurement.

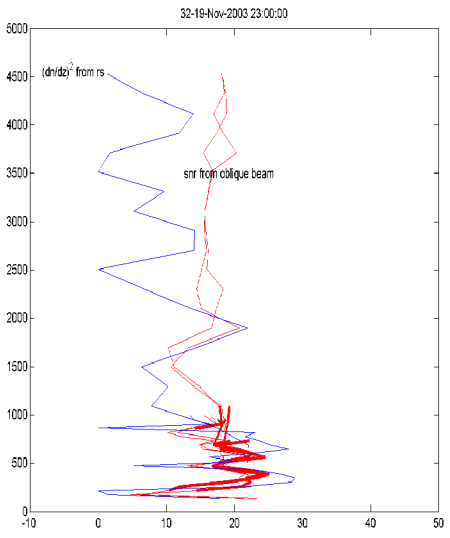

Figure 26: Same as figure 26, but the 19/11/03, 11:00 UTC.

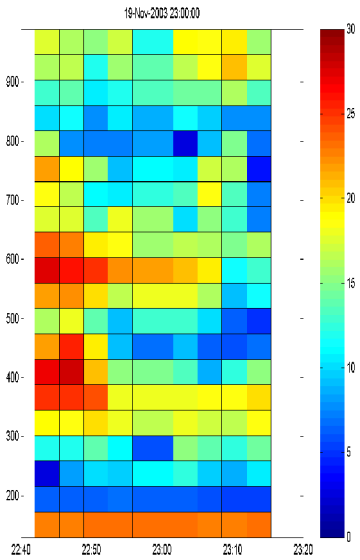

Figure 27: same as figure 27 but the 19/11/03, 11:00 UTC.

4.2. The Gossard formulation

According to Gossard, other terms than the signal to noise ratio, have to be taken into account in the comparison with the radiosonde. Gossard et al. (1982) derived a relationship between the turbulent structure parameters of the potential refractive index C_n^2, the turbulent structure parameter of the vertical speed C_w^2, and the mean property of the layer where it can be assumed that the turbulence is homogeneous and isotropic.

$$\left(\frac{dn}{dz}\right)^2 = \left(\frac{L_w}{L_n}\right)^{4/3} \left(\frac{dV_h}{dz}\right)^2 \frac{C_n^2}{C_w^2}$$

$$C_w^2 = B_w \varepsilon^{2/3}$$

Where: n is the potential refractive index defined in Gossard (1982), B_w a Kolmogorov constant, L_w and L_n are the mixing length scales for potential refractive index and vertical speed. These two quantities are not constant and depend on the stability, but Gossard et al. (1982) suggested that their ratio should be nearly constant because the same eddy ensemble mixes both quantities. Nevertheless, in 1998, he suggests that this ratio can vary in particular in very stable conditions, with values ranging form 2 to 6. He also suggested that in such case the isotropy of the turbulence might not be true. Such variation might prevent a quantitative evaluation of the gradient of the refractive index in case of strong inversion.

C_n^2 is linked to the signal to noise ratio though the radar equation. C_w^2 can be linked to the spectral width (corrected from the beam broadening) through the White formulation (Eqn. 2). $(dV_h/dz)^2$ is the square of the vertical shear of the mean horizontal wind, call thereafter shear^2.

For the 2 of December the signal to noise ratio follows rather well the evolution of $(dn/dz)^2$ computed from the radiosonde (Figure 28) but scaling the signal to noise ratio by a factor will not allow the value at 1000 m and the value at 500 m to coincide with the gradient of the refractive index computed from the radiosonde. From the wind profiler data the shear^2 and C_w^2 (Figure 29 and Figure 30) have been computed using the value which have passed the quality control.

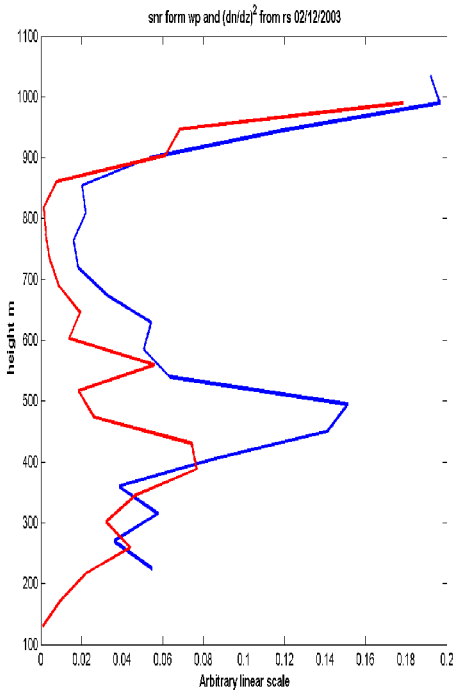

Figure 28: SNR from wind profiler (blu line), $(dn/dz)^2$ computed from the radiosonde (red line) using Gossard formulation. Arbitrary linear scale. 02/12/2003, 23:00 UTC

C_w^2 doesn't seem to indicate, a more turbulent layer at 1000 m than at 500 m, so the turbulence doesn't explain why the signal is stronger at 1000 than at 500 m. The shear appears to be smaller at 1000 m than at 500 m and so the change in the refractive index has to be increased at 500m. The correction using the shear, the width, and the signal to noise ratio indeed increase the gradient of the refractive index but the increase is now too strong (Figure 31). The result obtained is worse than the simple use of the signal to noise ratio. Compared to the radiosonde wind, the value for the shear obtained (Figure 29) from the wind profiler are high. In fact, after the quality control, only three points enter the average, so it is possible that, due to the lack of average, the variability in the winds is not reduced, resulting in high values for the shear. Other attempts have been done to quantify dn/dz for other cases but without success, mainly because too few data were able to pass the quality control.

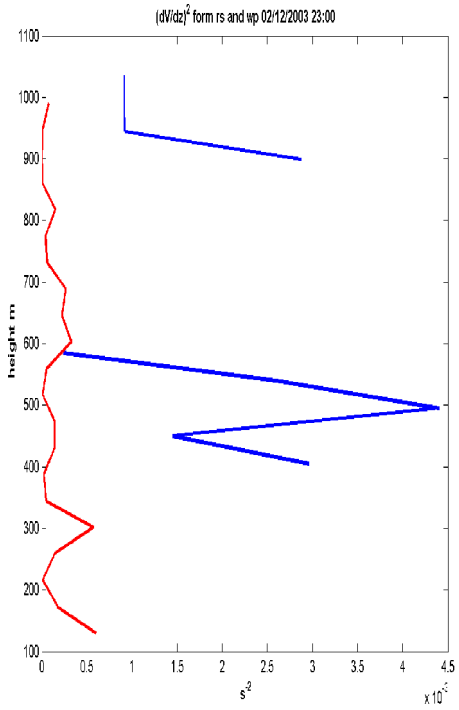

Figure 29: Shear^2(s^{-2}) red curve from radiosonde wind, blue curve from wind profiler wind, 02/12/2003, 23:00 UTC.

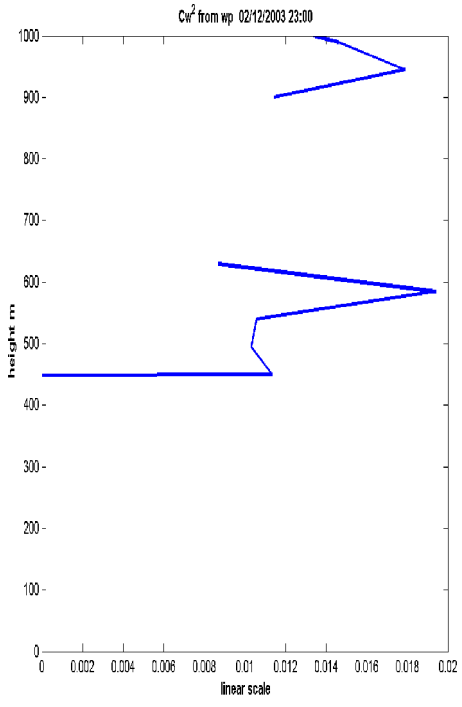

Figure 30: C_w^2 ($m^{4/3}s^{-2}$)computed from the corrected width, the volume filtering is taken into account through the White formulation, 02/12/2003, 23:00 UTC.

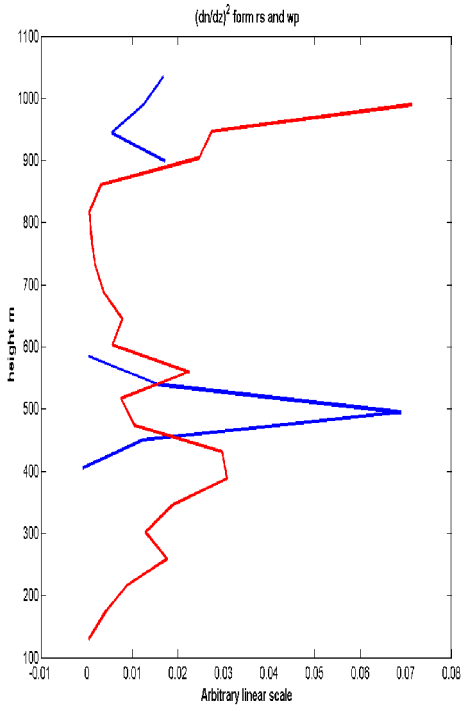

Figure 31: $(dn/dz)^2$ computed from the radiosonde, in red. Blue line indicates the wind profiler estimate of $(dn/dz)^2$, using Gossard formulation. Arbitrary linear scale, 02/12/2003, 23:00 UTC.

5. CONCLUSION AND FUTHER WORK

The analysis of the data reveals that the ground clutter and DC removal algorithm are affecting both the SNR and the width. The vertical beam is the most affected. Using basic quality control as realistic speed and width, spatial and temporal continuity, the variability in the SNR and in the width remains high, part of it is due to the atmosphere variability, but part of it is due to contamination by drizzle, ground clutter and associated algorithm. An average over ½ hour reduces significantly the variability of the SNR. For the corrected width, ½ hour average reduces as well the variability, but the correlation between different beams is remain small (0.75 for the two oblique beams). The comparison of the SNR with the radiosonde is encouraging. Strong signal in the wind profiler are clearly associated with variation in the refractive index. The variability in the SNR, which is partly due to the atmosphere variability, shows the difficulty in comparing a spot measurement with measurement integrated in time and space. On this data set, using the manufacturer software and some additional quality controls, a quantitative evaluation of the gradient of the refractive index has not been successful yet. Not enough data were able to pass the quality control, so the averaging process couldn't reduce the variability.

More complex data analyses are available like NIMA, from NCAR, and multipeak software, from Vaisala. By using more than one peak in the spectrum, using temporal and spatial continuity to score the selection, these software can compute all the moments. In their respective works, Stankov (2003) and Bianco (2005) mentioned the importance of using advanced data analysis to get information on the humidity structure. A reanalysis of the data will be done and different software will be evaluated.

A better protection from ground clutter should be done. The choice of suitable site for the wind profiler is important.

Technique like wavelet package could be used to remove DC, and ground clutter on the time series.

6. REFERENCES

Bianco L., D. Cimini, F. S. Marzano, and R. Ware, 2005: Combining Microwave Radiometer and Wind Profiler Radar Measurements for High-Resolution Atmospheric Humidity Profiling, *J. Atmos. Oceanic Technol.*, accepted for publication, 2005.

Doviak, R. J. and D. S Zrnic, 1984: Doppler radar and weather observations. Academic Press, 458 pp.

Frisch, A. S. and S. F. Clifford, 1974: A study of convection capped by a stable layer using Doppler radar and acoustic echo sounders, *J. Atmos. Sci.*, **31**, 1622-1628.

Furumoto, J., M. Kurimoto, and T. Tsuda, 2003: Continuous observations of humidity profiles with the MU radar-RASS combined with GPS and radiosonde measurements, *J. Atmos. Oceanic Technol.*, **1**, 23-41.

Gossard E. E., R. B. Chadwick, W. D. Neff and K. P. Moran, 1982: The use of ground-based Doppler Radars to measure gradients, fluxes and structure parameters in elevated layers, *J. of Applied Meteorology*, **21**, 211-226.

Gossard E. E., D. E. Wolfe, K. P Moran, R. A.Paulus, K. D. Anderson L.T. Rogers, 1998: Measurement of clear-air gradients and turbulence properties with Radar wind profilers, *J. Atmos. Oceanic Technol.*, **15**, 321-342.

Jacoby-Koaly, S., B. Campistron, S. Bernard, B. Benech, F. Ardhuin-Girard, J. Dessens, E. DuPont, and B. Carissimo, 2002: Turbulent dissipation rate in the boundary layer via UHF wind profiler Doppler spectral width measurements, *Boundary Layer Meteorol.*, **103**, 361-389.

Riddle, A.C., and W.M Angevine, 1992: Ground clutter removal from profiler spectra. Proc. 5th workshop on Technical and Scientific Aspect of MST radar, edited by B. Edwards SCOSTEP Secr, Urbana, III, 418-420.

Stankov B. B., E. R. Weswater, and E. E. Gossard, 1996: Use of wind profiler estimates of significant moisture gradients to improve humidity profile retrieval, *J. Atmos. Oceanic Technol.*, **13**, 1285-1290.

Stankov B. B, E. E. Gossard, B. L. Weber, R. J. Lataitis, A. B. White, D. E. Wolfe, D. C. Welsh, R. G. Strauch, 2003: Humidity gradient profiles from wind profiling radars using the NOAA/ETL advanced signal processing system (SPS), *J. Atmos. Oceanic Technol.*, **20**, 3-22.

White A. B., R. J Lataitis, R. S. Lawrence, 1999: Space and time filtering of remotely sensed velocity turbulence, *J. Atmos. Oceanic Technol.*, **16**, 1967-1972.